PERGAMON

Acta mater. Vol. 47, No. 7, pp. 2153–2164, 1999

Printed in Great Britain
PII: S1359-6454(99)00076-2
1359-6454/99 $20.00 + 0.00

THEORY OF INDENTATION OF PIEZOELECTRIC MATERIALS

A.E. GIANNAKOPOULOS† and S. SURESH

Department of Materials Science and Engineering, Massachusetts Institute of Technology, Cambridge, MA 02139, U.S.A.

(Received 19 December 1998; accepted 19 February 1999)

Abstract—A general theory is presented for the axisymmetric indentation of piezoelectric solids within the context of fully coupled, transversely isotropic elasticity models. Explicit expressions for *P–h* curves are derived for spherical, conical as well as cylindrical punch indenter geometries in a manner that can be directly related to the experimental measurements. In addition, results for different electrical boundary conditions that employ conducting or insulating indenters are also presented. The theory reveals that the indentation load vs penetration depth, and the contact area vs penetration depth relations have the same mathematical structure as the classical elastic indentation problem. It is, however, demonstrated that the electric field induced during indentation as a result of the electrical–mechanical coupling can resist or aid in the penetration of the indenter into the piezoelectric material depending on the electrical conductivity of the indenter and the surface boundary conditions of the indented substrate. It is also shown that the piezoelectric material exhibits pile-up or sink-in of material around the indenter as a consequence of electromechanical coupling, despite the absence of any inelastic deformation processes or strain hardening. The theoretical predictions are corroborated with detailed finite-element simulations for different indenter geometries. The theoretical results facilitate the prediction of some transient electrical effects which can be used in conjunction with experiments for the estimation of some of the elastic, dielectric and piezoelectric constants during instrumented indentation. Specific examples and details of such applications are addressed in separate papers. © *1999 Acta Metallurgica Inc. Published by Elsevier Science Ltd. All rights reserved.*

Keywords: Indentation; Ceramics, functional; Electric properties, piezoelectricities; Mechanical properties, elastic; Theory and modeling

1. INTRODUCTION

Theories of indentation of elastic and elastoplastic materials and their applications to the mechanical design, characterization and testing of materials have been topics of interest to engineers and scientists for well over a century (e.g. Refs [1–3]). With the rapid expansion of modern materials engineering, there is, however, a growing list of non-traditional materials which are increasingly used for their fully coupled, mechanical–nonmechanical characteristics. Piezoelectric solids represent a broad class of materials whose electrical–mechanical coupling has led to important engineering applications in such products as sensors, actuators and "smart" structures (e.g. Ref. [4]).

Indentation of piezoelectric solids represents a topic of considerable scientific and technological interest on many accounts. (1) Piezoelectric materials are used in some "contact-prone" applications, wherein indentation analysis would provide the basic foundation for developing an understanding of the mechanics of contact. (2) With the advent of sophisticated instrumented indenters, probing of materials at the macro-, micro-, and nano-scales is fast becoming a tool for the testing of material properties (e.g. Refs [5–7]). Instrumented indentation can potentially offer a powerful new tool for the characterization of the mechanical and electrical properties of piezoelectric materials in thin-film and bulk form. (3) As shown later in this work and in companion papers [8, 9], a continuous record of some mechanical and electrical responses during instrumented indentation can serve as a guide for monitoring such characteristics as the poling direction, ageing response and activation energy for depolarization.

There have been some prior attempts at the development of continuum solutions for the indentation of piezoelectric solids for a limited set of indenter geometries and indentation boundary conditions [10]. To date, however, no general theory of indentation has been reported for piezoelectric materials where the "forward" problem of indentation mechanics and the "inverse" problem of property characterization have been fully addressed for different geometries of indenters that are commercially available. It is also desirable to develop a theory which provides explicit analytical expressions linking the key par-

†To whom all correspondence should be addressed.

ameters of indentation, such as the indentation force, P, as a function of the depth of penetration, h, of the indenter into the material, which can be directly measured in experiments.

Motivated by these considerations, the objective of the present work was to develop a general theory for the axisymmetric indentation of piezoelectric solids within the context of fully coupled, transversely isotropic elasticity models. The governing equations and the formulation of the boundary value problem for general axisymmetric indenters of spherical, conical and cylindrical punch geometries are outlined in Section 2. Theoretical results for the flat-end axisymmetric cylindrical punch, conical indenter and spherical indenter are then presented in Section 3, for different electrical boundary conditions. In this section, explicit expressions for P–h curves are derived in a manner that can be directly related to the experimental measurements. Section 4 provides numerical corroboration of the theory by recourse to finite-element analyses. The paper concludes with Section 5 with a summary of findings.

2. THEORETICAL FORMULATION

2.1. Basic geometry and nomenclature

Consider the planar surface of a piezoelectric material which is normally contacted by an axisymmetric indenter, as shown in Figs 1(a)–(c). The in-plane dimensions and the thickness of the indented material (normal to the indented surface) are much larger (i.e. at least six times larger) than the diameter, $2a$, of the largest imprint made on it by the indenter. In the cylindrical coordinate system employed in Fig. 1, the in-plane radial direction is denoted by r, while the out-of-plane direction by z; at the indented surface, $z = 0$. The in-plane angular position is denoted by θ. The depth of penetration of the indenter into the substrate is h, in response to the indentation force P. The axis of polarization of the indented piezoelectric material coincides with the z axis. In the following discussion of material properties, the subscripts "3" denote properties along the poling direction whereas the subscripts "1" and "2" represent those in two mutually orthogonal in-plane directions.

The process modelled here represents quasi-static, frictionless, normal indentation of a transversely isotropic, piezoelectric material by an axisymmetric rigid indenter. Planar isotropy along the poled axis (z axis) is assumed with the result that an electric field parallel to the poling axis interacts in the same way with the axial stress along any radial direction. Similarly, an electric field parallel to any in-plane radial direction interacts in the same way with a shear stress σ_{rz} in the corresponding rz-plane. The shear strain in the 1–2 plane (i.e. the plane of the indented surface) is not excited piezoelectrically. The present analysis deals with small strains and small electric displacements.

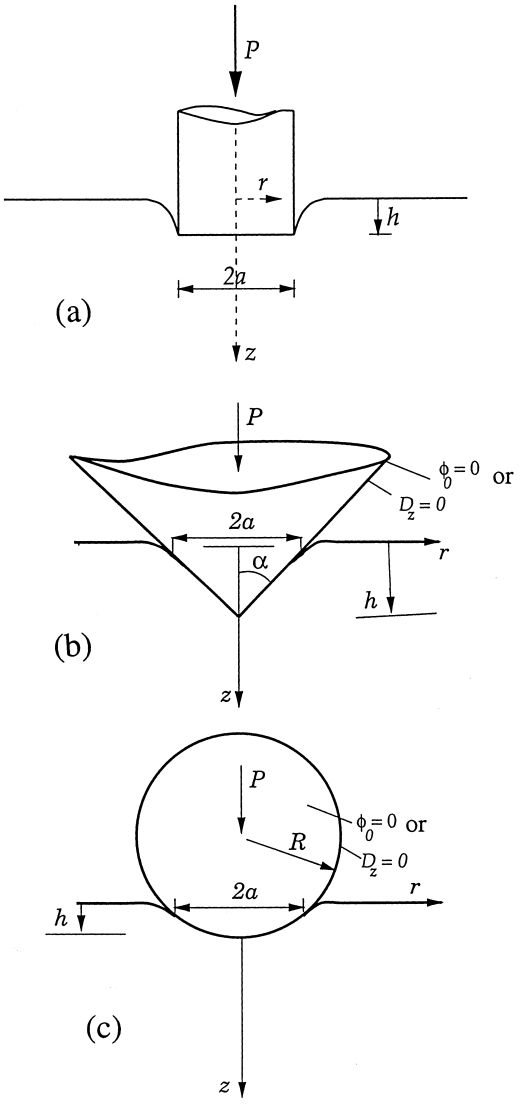

Fig. 1. Schematic of the normal indentation of piezoelectric materials. (a) Flat-ended cylindrical punch. (b) Conical indenter. (c) Spherical indenter.

2.2. Governing equations

In the absence of body and inertia forces, the equilibrium equations, written in terms of stress components σ_{ij}, are:

$$\frac{\partial \sigma_{rr}}{\partial r} + \frac{\partial \sigma_{rz}}{\partial z} + \frac{\sigma_{rr} - \sigma_{\theta\theta}}{r} = 0,$$

$$\frac{\partial \sigma_{rz}}{\partial r} + \frac{\partial \sigma_{zz}}{\partial z} + \frac{\sigma_{rz}}{r} = 0. \quad (1)$$

The geometric conditions which relate small strains and displacements are

$$\epsilon_{rr} = \frac{\partial u_r}{\partial r},\ \epsilon_{\theta\theta} = \frac{u_r}{r},\ \epsilon_{zz} = \frac{\partial u_z}{\partial z},\ \gamma_{rz} = \frac{\partial u_r}{\partial z} + \frac{\partial u_z}{\partial r} \quad (2)$$

where ϵ_{ij} are the components of the strain tensor and u_i are the components of the displacement vector. The Maxwell electrostatic equation, in the absence of volume electric charges, is

$$\frac{\partial D_r}{\partial r}+\frac{D_r}{r}+\frac{\partial D_z}{\partial z}=0 \tag{3}$$

where $D_r(r,z)$ and $D_z(r,z)$ are the radial and axial electric displacements, respectively. The Gauss equations give the electric flux vector

$$E_r=-\frac{\partial \phi}{\partial r},\ E_z=-\frac{\partial \phi}{\partial z} \tag{4}$$

where $\phi(r,z)$ is the electric potential. In the absence of thermal strains, the constitutive equations of linear piezoelectricity (the so-called Duhamel–Neumann relations) are

$$\sigma_{rr}=c_{11}\epsilon_{rr}+c_{12}\epsilon_{\theta\theta}+c_{13}\epsilon_{zz}-e_{31}E_z,$$

$$\sigma_{\theta\theta}=c_{12}\epsilon_{rr}+c_{11}\epsilon_{\theta\theta}+c_{13}\epsilon_{zz}-e_{31}E_z \tag{5a}$$

$$\sigma_{zz}=c_{13}\left(\epsilon_{rr}+\epsilon_{\theta\theta}\right)+c_{33}\epsilon_{zz}-e_{33}E_z,$$

$$\sigma_{rz}=c_{44}\gamma_{rz}-e_{15}E_r \tag{5b}$$

where c_{ij} are the elastic constants for constant electric flux, and e_{ij} are the piezoelectric constants for transverse isotropy. Note that any pre-existing residual stresses or strains do not have any effect on elastic indentation.

The electric displacements are influenced by the strains and the electric fluxes according to the relations

$$D_r=e_{15}\gamma_{rz}+\varepsilon_{11}E_r,$$

$$D_z=e_{31}\left(\epsilon_{rr}+\epsilon_{\theta\theta}\right)+e_{33}\epsilon_{zz}+\varepsilon_{33}E_z \tag{6}$$

where ε_{ii} are the dielectric constants for transverse isotropy at constant strain. Substituting equations (3)–(5a), (5b) and (6) into equations (1) and (2), we obtain the reduced problem in terms of the principal quantities (u_r, u_z, ϕ):

$$c_{11}\left(\frac{\partial^2 u_r}{\partial r^2}+\frac{1}{r}\frac{\partial u_r}{\partial r}-\frac{u_r}{r^2}\right)+c_{44}\frac{\partial^2 u_r}{\partial r^2}+\left(c_{13}+c_{44}\right)\frac{\partial^2 u_z}{\partial r\partial z}+\left(e_{31}+e_{15}\right)\frac{\partial^2 \phi}{\partial r\partial z}=0 \tag{7}$$

$$c_{44}\left(\frac{\partial^2 u_z}{\partial r^2}+\frac{1}{r}\frac{\partial u_z}{\partial r}\right)+c_{33}\frac{\partial^2 u_z}{\partial z^2}+\left(c_{13}+c_{44}\right)\frac{\partial}{\partial z}\left(\frac{\partial u_r}{\partial r}+\frac{u_r}{r}\right)+e_{15}\left(\frac{\partial^2 \phi}{\partial r^2}+\frac{1}{r}\frac{\partial \phi}{\partial r}\right)+e_{33}\frac{\partial^2 \phi}{\partial z^2}=0 \tag{8}$$

$$e_{15}\left(\frac{\partial^2 u_z}{\partial r^2}+\frac{1}{r}\frac{\partial u_z}{\partial r}\right)+e_{33}\frac{\partial^2 u_z}{\partial z^2}+\left(e_{15}+e_{31}\right)\frac{\partial}{\partial z}\left(\frac{\partial u_r}{\partial r}+\frac{u_r}{r}\right)-\varepsilon_{11}\left(\frac{\partial^2 \phi}{\partial r^2}+\frac{1}{r}\frac{\partial \phi}{\partial r}\right)-\varepsilon_{33}\frac{\partial^2 \phi}{\partial z^2}=0. \tag{9}$$

2.3. Formulation of the boundary value problem

The rigid axisymmetric indenters considered here include the flat-ended cylindrical punch, sphere and circular cone. For each of these indenter geometries, two electrical states are examined (Fig. 1): (a) the indenter is a perfect electric insulator with a known radial distribution of electric charge at its surface; and (b) the indenter is a perfect electric conductor with a known radial distribution of electric potential at its surface. The monotonically advancing contact, which is a circular disc of radius a, between the indenter and the substrate, is non-conforming.

2.3.1. Mechanical boundary conditions. The mechanical displacements u_r and u_z, and the electric potential ϕ are required, for all the indenter geometries, to have continuous second derivatives, and to vanish at distances far away from the contact region, i.e. $u_r,\ u_z,\ \phi \to o(1/\sqrt{z^2+r^2}) \to 0$ as $\sqrt{z^2+r^2} \longrightarrow \infty$. Inside the contact area, $0 \le r \le a$, the mechanical boundary conditions must satisfy the applied displacements. This condition implies that for the flat-ended cylindrical punch, Fig. 1(a), $u_z(r,0) = h$. For a conical indenter with an included apex angle 2α, Fig. 1(b), and for the spherical indenter with a diameter $2R$, respectively,

$$u_z(r,0)=h-(a-r)\cot\alpha \text{ (cone)};$$

$$u_z(r,0)=h-\frac{r^2}{2R} \text{ (sphere)}. \tag{10}$$

For all three indenters,

$$\sigma_{rz}(r,0)=0;\ r\ge 0,\ \sigma_{zz}(r,0)=0;\ r>a. \tag{11}$$

For a smooth transition of deformation at the contact perimeter ($r = a$), the continuity condition should hold such that $\sigma_{zz}(a,0) = 0$. The first of the expressions in equation (11) indicates the absence of frictional or other applied shear tractions, whereas the latter indicates the absence of any applied normal loads outside the contact region.

2.3.2. Electrical boundary conditions. When all three indenters are perfect electrical conductors with a constant potential ϕ_0,

$$\phi(r,0)=\phi_0 \text{ for } 0\le r<a,\ D_z(r,0)=0 \text{ for } r>a. \tag{12}$$

The first of these equations indicates that the potential of the indenter is also the potential of the substrate within the contact area, whereas the second

equation shows that the electric charge distribution outside the contact area is zero.

When all three indenters are perfect electrical insulators with a zero electric charge distribution,

$$D_z(r,0) = 0;\ r \geq 0. \tag{13}$$

Equation (13) indicates that the electric charge distribution of the surface is zero. The above conditions reduce to two well-posed, mixed boundary value problems which have unique solutions.

2.4. General solution to the boundary value problem

In view of the axisymmetry of the problem, Hankel-type integral transformations are employed to derive a general solution. For this purpose, consider the transformation of mechanical displacements and electrical potential with respect to the radial direction r: $(u_r,\ u_z,\ \phi) \rightarrow (\bar{u}_r(\xi,z),\ \bar{u}_z(\xi,z),\ \bar{\phi}(\xi,z))$ [11]. Now apply the integral transformation, $\int_0^\infty J_1(\xi r)\mathrm{d}r$ on equation (7) and $\int_0^\infty J_0(\xi r)\mathrm{d}r$ on equations (8) and (9), where J_0 and J_1 are the zeroeth and first-order Bessel functions, respectively, and ξ is the radial coordinate in the transformed space. Then, the partial differential equations (7)–(9) tranform to a homogeneous system of ordinary differential equations of $\bar{u}_r(\xi,z)$, $\bar{u}_z(\xi,z)$ and $\bar{\phi}(\xi,z)$, with respect to z. There are three ordinary equations with three unknowns; hence, from standard methodology, a general exponential form, $\mathrm{e}^{-k\xi z}$, of the solution for the transformed principal variables results. The parameter k must satisfy the characteristic (3×3) determinant of the system of ordinary differential equations

$$\det[a_{ij}] = 0. \tag{14}$$

The same equations were derived in Ref. [12] using a different method involving potential theory, for some aspects of the point force indentation problem. The characteristic equation [equation (14)] is of sixth order and has two real roots, $k = \pm k_1$ and four complex roots $k = \pm(\delta \pm \mathrm{i}\omega)$ $(\mathrm{i} = \sqrt{-1})$. Here, it is assumed that all roots are distinct (without loss of generality, k_1, δ are taken positive definite and ω non-negative). In order to satisfy the regularity condition, i.e. $u_r,\ u_z,\ \phi \rightarrow \mathrm{o}(1/\sqrt{z^2+r^2}) \rightarrow 0$ as $\sqrt{z^2+r^2} \longrightarrow \infty$, we select $k = k_1$ as the real root. k_1, δ, ω can then be found by simplifying the coefficients a_{ij} (e.g. Ref. [10])

$$a_{11} = c_{44}k^2 - c_{11},\ a_{12} = -a_{21} = (c_{13} + c_{44})k,$$

$$a_{22} = c_{33}k^2 - c_{44},\ a_{13} = a_{31} = -(e_{31} + e_{15})k_1,$$

$$a_{23} = -a_{32} = -e_{33}k^2 + e_{15},$$

$$a_{33} = \varepsilon_{33}k_1^2 - \varepsilon_{11}. \tag{15}$$

Evaluating the coefficients a_{ij} for $k = k_1$, the following parameters are defined:

$$\alpha_1 = a_{12}a_{23} - a_{13}a_{22},\ \beta_1 = -a_{11}a_{23} - a_{12}a_{13},$$

$$\gamma_1 = a_{11}a_{22} + a_{12}^2. \tag{16}$$

Then, the additional constants $\alpha_{21},\ldots,\gamma_{22}$ are obtained from δ and ω through the complex identities

$$\alpha_{21} + \mathrm{i}\alpha_{22} = \alpha_1(\delta + \mathrm{i}\omega),\ \beta_{21} + \mathrm{i}\beta_{22} = \beta_1(\delta + \mathrm{i}\omega),$$

$$\gamma_{21} + \mathrm{i}\gamma_{22} = \gamma_1(\delta + \mathrm{i}\omega). \tag{17}$$

Taking into account the regularity condition again, the Hankel-transformed solution is

$$\begin{aligned}\bar{u}_r(\xi,z) = {} & \alpha_1 A_1(\xi)\mathrm{e}^{-k_1\xi z} + \big(\alpha_{21}A_2(\xi) \\ & - \alpha_{22}A_3(\xi)\big)\mathrm{e}^{-\delta\xi z}\cos(\omega\xi z) \\ & + \big(\alpha_{22}A_2(\xi) \\ & + \alpha_{21}A_3(\xi)\big)\mathrm{e}^{-\delta\xi z}\sin(\omega\xi z)\end{aligned} \tag{18}$$

$$\begin{aligned}\bar{u}_z(\xi,z) = {} & \beta_1 A_1(\xi)\mathrm{e}^{-k_1\xi z} + \big(\beta_{21}A_2(\xi) \\ & - \beta_{22}A_3(\xi)\big)\mathrm{e}^{-\delta\xi z}\cos(\omega\xi z) \\ & + \big(\beta_{22}A_2(\xi) \\ & + \beta_{21}A_3(\xi)\big)\mathrm{e}^{-\delta\xi z}\sin(\omega\xi z)\end{aligned} \tag{19}$$

$$\begin{aligned}-\bar{\phi}(\xi,z) = {} & \gamma_1 A_1(\xi)\mathrm{e}^{-k_1\xi z} + \big(\gamma_{21}A_2(\xi) \\ & - \gamma_{22}A_3(\xi)\big)\mathrm{e}^{-\delta\xi z}\cos(\omega\xi z) \\ & + \big(\gamma_{22}A_2(\xi) \\ & + \gamma_{21}A_3(\xi)\big)\mathrm{e}^{-\delta\xi z}\sin(\omega\xi z).\end{aligned} \tag{20}$$

The functions $A_1(\xi)$, $A_2(\xi)$, $A_3(\xi)$ have to be determined from the boundary conditions. Inverting the Hankel transforms we obtain the general representation of the solution. It is clear that all mechanical and electrical constants interact through the characteristic equation, equation (14), in a very complex way. For the uncoupled problem, for $e_{ij} = 0$, we recover separately the classic, transversly isotropic, purely mechanical conical indentation [13], or spherical indentation [14], and the rigid dielectric electrostatic results [15].

The solution at the surface ($z = 0$) can be represented in a general form as

$$\begin{aligned}u_z(r,0) = \int_0^\infty & \big(\beta_1 A_1(\xi) + \beta_{21}A_2(\xi) \\ & - \beta_{22}A_3(\xi)\big)J_0(\xi r)\mathrm{d}\xi\end{aligned} \tag{21}$$

$$\begin{aligned}\sigma_{rz}(r,0) = \int_0^\infty & \big(m_1 A_1(\xi) + m_2 A_2(\xi) \\ & - m_3 A_3(\xi)\big)\xi J_1(\xi r)\mathrm{d}\xi\end{aligned} \tag{22}$$

$$\sigma_{zz}(r,0)=\int_0^\infty\left(\frac{m_1}{k_1}A_1(\xi)+\frac{m_2\delta+m_3\omega}{\delta^2+\omega^2}A_2(\xi)-\frac{m_3\delta-m_2\omega}{\delta^2+\omega^2}A_3(\xi)\right)\xi J_0(\xi r)\mathrm{d}\xi \tag{23}$$

$$\phi(r,0)=-\int_0^\infty\left(\gamma_1A_1(\xi)+\gamma_{21}A_2(\xi)-\gamma_{22}A_3(\xi)\right)J_0(\xi r)\mathrm{d}\xi \tag{24}$$

$$D_z(r,0)=\int_0^\infty\left(\frac{m_4}{k_1}A_1(\xi)+\frac{m_5\delta+m_6\omega}{\delta^2+\omega^2}A_2(\xi)-\frac{m_6\delta-m_5\omega}{\delta^2+\omega^2}A_3(\xi)\right)\xi J_0(\xi r)\mathrm{d}\xi \tag{25}$$

where the constants m_i are defined in Appendix A. The solution at regions far away from the indented area $\left(\sqrt{z^2+r^2}\longrightarrow\infty\right)$ tend asymptotically to the point force and point charge results [12].

For frictionless contact, the shear stress at the surface is zero [$\sigma_{rz}(r,0)=0$]. Then, since $m_3\neq 0$, equation (22) gives

$$A_3(\xi)=\frac{m_1}{m_3}A_1(\xi)+\frac{m_2}{m_3}A_2(\xi) \tag{26}$$

which eliminates the $A_3(\xi)$ function. The remaining unknown functions $A_1(\xi)$ and $A_2(\xi)$ can be found from the surface electrical and mechanical boundary conditions. Such solutions will be described, for the different electrical boundary conditions, for the three indenter geometries in Section 3.

Some general results can be found from the boundary conditions at the surface ($z=0$). The second part of equation (5b) gives $\gamma_{rz}=e_{15}E_r/c_{44}$, indicating that the shear strain at the surface is not zero, although the shear stress is. At the surface and away from the contact perimeter ($r\geq a$), $\sigma_{zz}(r,0)=0$ and $D_z(r,0)=0$. Then, equations (5b) and (6) give

$$\left(\epsilon_{rr}+\epsilon_{\theta\theta}\right)\left(c_{13}\varepsilon_{33}+e_{31}e_{33}\right)+\epsilon_{zz}\left(c_{33}\varepsilon_{33}+e_{33}e_{33}\right)=0. \tag{27}$$

For typical piezoelectric ceramics, $(c_{13}\varepsilon_{33}+e_{31}e_{33})>0$, $(c_{33}\varepsilon_{33}+e_{33}e_{33})>0$ and $\epsilon_{zz}<0$. Therefore, $(\epsilon_{rr}+\epsilon_{\theta\theta})>0$, indicating that tensile strains develop outside the contact area at the surface. Such tensile strains may be reduced if a tensile axial and/or a compressive radial pre-strain due to electrical or mechanical loading are present. Alternatively, the surface tensile strains could be reduced, if the ratio of the material constant $(c_{33}\varepsilon_{33}+e_{33}e_{33})/(c_{13}\varepsilon_{33}+e_{31}e_{33})$ is minimized.

3. GENERAL RESULTS

We now outline the general theoretical results for the three indenter geometries shown in Fig. 1 for the two boundary conditions involving the conducting or the insulated indenter. The results are derived in closed form for the following general quantities: indenter penetration depth into the substrate, h; contact pressure, $p(r)$ [which at the indented surface is simply equal to $-\sigma_{zz}(r,0)$ for $0\leq r\leq a$]; the resultant force, P, which can be found by integrating $p(r)$ such that

$$P=2\pi\int_0^a rp(r)\mathrm{d}r \tag{28}$$

and the displacements, $u_z(a,0)$, at the contact perimeter which account for the pile-up [$u_z(a,0)>0$] or sink-in [$u_z(a,0)<0$] of the material around the indenter. In addition, the following specific quantities are derived for the case of a conducting indenter: the electric charge distribution under the indenter, $q(r)=-D_z(r,0)$ $(0\leq r\leq a)$; and the total electric charge, Q, under the indenter which can be found by integrating $q(r)$:

$$Q=2\pi\int_0^a rq(r)\mathrm{d}r. \tag{29}$$

For the insulated indenter, on the other hand, the electric potential distribution at the surface within the contact area, $\phi(r,0)$, was also computed.

Table 1 shows the derived expressions for h, $p(r)$, P, $u_z(a,0)$, $q(r)$ and Q, in terms of the various material constants and indenter geometrical dimensions defined previously, for the poled piezoelectric solid which is indented by a conducting cylindrical punch, cone or sphere. Table 2 shows the corresponding expressions for h, $p(r)$, P, $u_z(a,0)$, and $\phi(r,0)$, for the poled piezoelectric solid which is indented by an insulated cylindrical punch, cone or sphere. (The constants M_1–M_{10} are defined in Appendix A.) Note that the results in Tables 1 and 2 reduce to the known mechanical indentation results, shown in Table 3, for transversely isotropic elastic solids indented by the punch, cone and sphere in the absence of any piezoelectric effect (i.e. when $M_3=0$ and $M_7=0$).

Additional features of the results of Tables 1 and 2, which are applicable to specific indenter geometries and boundary conditions, are given below. All the results reported in Tables 1 and 2 as well as in the following subsections reduce to the known results [12] for the indentation of piezoelectric materials by a point force or point charge at regions far away from the indenter contact area, i.e. for $(r^2+z^2)\gg a^2$.

3.1. Flat-ended cylindrical punch

3.1.1. Conducting indenter. For the flat-ended punch, the penetration depth h remains uniformly the same within the contact area (Table 1). The surface deformation outside the contact perimeter, however, varies with radial distance as

Table 1. Poled substrate–conducting indenter

(flat)	$h = \text{constant}$
(conical)	$h = \frac{1}{2}[\pi a \cot\alpha] + \frac{M_1M_6 - M_2M_5}{M_4M_5 - M_3M_6}\phi_0$
(spherical)	$h = \frac{a^2}{R} + \left[\frac{M_1M_6 - M_2M_5}{M_4M_5 - M_3M_6}\right]\phi_0$
(flat)	$p(r) = \frac{2h(M_5M_4 - M_6M_3) - 2\phi_0(M_6M_1 - M_2M_5)}{\pi(M_1M_4 - M_2M_3)\sqrt{a^2 - r^2}}$
(conical)	$p(r) = \cot\alpha\left[\frac{M_4M_5 - M_3M_6}{M_1M_4 - M_2M_3}\right]\operatorname{arccosh}\frac{a}{r}$
(spherical)	$p(r) = \frac{4}{\pi R}\left[\frac{M_4M_5 - M_3M_6}{M_1M_4 - M_2M_3}\right]\sqrt{a^2 - r^2}$
(flat)	$P = 4a\left[\frac{h(M_5M_4 - M_6M_3) - \phi_0(M_6M_1 - M_2M_5)}{(M_1M_4 - M_2M_3)}\right]$
(conical)	$P = \pi a^2 \cot\alpha\left[\frac{M_4M_5 - M_3M_6}{M_1M_4 - M_2M_3}\right]$
(spherical)	$P = \frac{8}{3}\left[\frac{M_4M_5 - M_3M_6}{M_1M_4 - M_2M_3}\right]\frac{a^3}{R}$
(flat)	$u_z(a,0) = h$
(conical)	$u_z(a,0) = \left(\frac{\pi}{2} - 1\right)a\cot\alpha + \left[\frac{M_1M_6 - M_2M_5}{M_4M_5 - M_3M_6}\right]\phi_0$
(spherical)	$u_z(a,0) = \frac{a^2}{2R} + \left[\frac{M_1M_6 - M_2M_5}{M_4M_5 - M_3M_6}\right]\phi_0$
(flat)	$q(r) = -\frac{2h(M_7M_4 - M_8M_3) - 2\phi_0(M_1M_8 - M_2M_7)}{\pi(M_1M_4 - M_2M_3)\sqrt{a^2 - r^2}}$
(conical)	$q(r) = \frac{2\phi_0(M_1M_8 - M_2M_7) - (M_7M_4 - M_8M_3)(2h - \pi a\cot\alpha)}{\pi\sqrt{a^2 - r^2}(M_1M_4 - M_2M_3)} + \cot\alpha\left[\frac{M_7M_4 - M_8M_3}{M_1M_4 - M_2M_3}\right]\operatorname{arccosh}\frac{a}{r}$
(spherical)	$q(r) = \frac{2\phi_0(M_1M_8 - M_2M_7) - (M_7M_4 - M_8M_3)(2h - 2a^2/R)}{\pi\sqrt{a^2 - r^2}(M_1M_4 - M_2M_3)} + \frac{4}{\pi R}\left[\frac{M_7M_4 - M_8M_3}{M_1M_4 - M_2M_3}\right]\sqrt{a^2 - r^2}$
(flat)	$Q = 4a\left[\frac{\phi_0(M_1M_8 - M_2M_7) - h(M_7M_4 - M_8M_3)}{(M_1M_4 - M_2M_3)}\right]$
(conical)	$Q = \pi a^2 \cot\alpha\left[\frac{M_7M_4 - M_8M_3}{M_1M_4 - M_2M_3}\right] + 2a\frac{2\phi_0(M_1M_8 - M_2M_7) - (M_7M_4 - M_8M_3)(2h - \pi a\cot\alpha)}{M_1M_4 - M_2M_3}$
(spherical)	$Q = \frac{16}{3}\left[\frac{M_7M_4 - M_8M_3}{M_1M_4 - M_2M_3}\right]\frac{a^3}{2R} + 4a\left[\frac{\phi_0(M_1M_8 - M_2M_7) - (M_7M_4 - M_8M_3)(h - a^2/R)}{M_1M_4 - M_2M_3}\right]$

$$u_z(r,0) = \frac{2}{\pi}h\arcsin\left\{\frac{a}{r}\right\} \text{ for } r \geq a. \tag{30}$$

The contact pressure exhibits the classic square root singularity of the uncoupled mechanical case at the contact perimeter. However, a mechanical displacement due to the potential ϕ_0 is additionally present, and the contact pressure is therefore modified due to the coupling.

For stability of mechanical loading, the resultant force should increase with increasing penetration such that $\partial P/\partial h \geq 0$, with zero only when $P = h = 0$. Then, the stability condition becomes

$$(M_5M_4 - M_6M_3) \times (M_4M_1 - M_2M_3) > 0. \tag{31}$$

Table 2. Poled substrate–insulating indenter

Quantity	Flat punch	Conical punch	Spherical punch
$h=$	constant	$\frac{\pi a \cot\alpha}{2}$	$\frac{a^2}{R}$
$p(r)=$	$\frac{2h(M_5M_8 - M_6M_7)}{\pi(M_1M_8 - M_2M_7)\sqrt{a^2 - r^2}}$	$\cot\alpha \frac{M_8M_5 - M_7M_6}{M_1M_8 - M_2M_7} \operatorname{arccosh}\frac{a}{r}$	$\frac{4}{\pi R}\frac{M_8M_5 - M_7M_6}{M_1M_8 - M_2M_7}\sqrt{a^2 - r^2}$
$P=$	$4a\frac{h(M_5M_8 - M_6M_7)}{(M_1M_8 - M_2M_7)}$	$\pi a^2 \cot\alpha \frac{M_8M_5 - M_7M_6}{M_1M_8 - M_2M_7}$	$\frac{8}{3}\frac{M_8M_5 - M_7M_6}{M_1M_8 - M_2M_7}\frac{a^3}{R}$
$u_z(a,0)=$	h	$\left(\frac{\pi}{2} - 1\right)a\cot\alpha$	$\frac{a^2}{2R}$
$\phi(r)=$	$\phi_q = \frac{h(M_3M_8 - M_4M_7)}{\pi(M_1M_8 - M_2M_7)}$	$\phi_q\left(\frac{\pi}{2}\cot\alpha - \frac{r}{a}\right)$	$\phi_q\left(2 - \frac{r^2}{a^2}\right)$

The contribution from the potential ϕ_0 acts either in favor of or against the normal indentation displacement h. For the particular case of

$$h(M_5M_4 - M_6M_3) = \phi_0(M_6M_1 - M_2M_5) \quad (32)$$

$p(r) = 0$, $P = 0$ (i.e. the net mechanical force is exactly countered by the resistance from the electric field) and the stresses under the indented surface are minimized. Conversely, even in the absence of an electric potential, an electric charge could accumulate at the surface due to the applied load or displacement. There is a combination of load and potential such that the electric charge does not exist under the punch:

$$h(M_7M_4 - M_8M_3) = \phi_0(M_8M_1 - M_2M_7). \quad (33)$$

Then, $q(r) = 0$, $Q = 0$ (i.e. the net electric charge is exactly countered by the resistance from the mechanical displacement).

The electric potential outside the contact perimeter is

$$\phi(r,0) = \frac{2}{\pi}\phi_0 \arcsin\left\{\frac{a}{r}\right\} \text{ for } r \geq a. \quad (34)$$

3.1.2. Insulated indenter. The surface deformation outside the contact area for this case is the same as that shown in equation (30). The contact pressure shows a square root singularity (Table 2).

A perfectly insulated indenter with zero distributed electric charge creates a constant electric potential, ϕ_q, inside the contact area. The electric potential outside the contact perimeter is similar to the perfect conductor case, equation (34).

For stability, $\partial P/\partial h \geq 0$, with zero only when $P = h = 0$. Then, the stability condition becomes

$$(M_5M_8 - M_7M_3)(M_8M_1 - M_2M_7) > 0. \quad (35)$$

3.2. Circular cone

3.2.1. Conducting indenter. The results shown in Tables 1 and 2 for the conical indenter were obtained directly using the Hankel transformation

Table 3. Uncoupled mechanical case

Quantity	Flat punch	Conical punch	Spherical punch
$h=$	constant	$\frac{\pi a \cot\alpha}{2}$	$\frac{a^2}{R}$
$p(r)=$	$\frac{2hM_5}{\pi M_1\sqrt{a^2 - r^2}}$	$\cot\alpha \frac{M_5}{M_1} \operatorname{arccosh}\frac{a}{r}$	$\frac{4}{\pi R}\frac{M_5}{M_1}\sqrt{a^2 - r^2}$
$P=$	$4a\frac{hM_5}{M_1}$	$\pi a^2 \cot\alpha \frac{M_5}{M_1}$	$\frac{8}{3}\frac{M_5}{M_1}\frac{a^3}{R}$
$u_z(a,0)=$	h	$\left(\frac{\pi}{2} - 1\right)a\cot\alpha$	$\frac{a^2}{2R}$

method described in Section 2. These results have also been derived, for an independent check, by linear superposition of the flat-punch solutions given in Tables 1 and 2. It can be shown that the surface values such as the contact pressure, the vertical and the radial displacements follow the same radial functional forms as those of the uncoupled mechanical indentation solution (Table 3), although the amplitudes are different.

For $\phi_0 = 0$, we recover the classic condition of linear elasticity, $h = \pi a \cot\alpha/2$. The additional part of the indentation depth is due to displacement induced by the constant potential, ϕ_0, of the indenter. Since

$$\operatorname{arccosh}\frac{a}{r} = \ln\frac{a+\sqrt{a^2-r^2}}{a-\sqrt{a^2-r^2}} \tag{36}$$

at the contact center ($r \to 0$), the contact stresses $p(r)$ have a logarithmic singularity.

The P–a dependence is the same as the uncoupled mechanical case. The P–h functional form also follows the classic mechanical result, $P \sim h^2$. Note that the indenter's electrical potential, ϕ_0, does not explicitly influence the applied load, P. For $\phi_0 = 0$, we recover the classic sink-in solution of the uncoupled mechanical solution, $u_z\ (a,0) = ((\pi/2)-1)a\cot\alpha$. However, a non-zero potential could lead to a pile-up or reduce the magnitude of sink-in from the pure mechanical case.

In addition to the electrical potential, the mechanical load also induces an electric charge under the indenter (Table 1). Note that the electric charge shows a square root singularity at the contact perimeter ($r = a$) and a logarithmic singularity at the center of contact ($r = 0$).

3.2.2. Insulated indenter. The relation between the penetration depth, h, and the contact radius, a, as well as the P–h relation are exactly as in the pure mechanical case. Since the potential is zero, the contact perimeter ($r = a$) always sinks in according to the pure mechanical result.

If the potential for the flat-ended cylindrical punch is ϕ_q, then at the center of contact of the conical indenter, the potential is given by

$$\phi(0,0) = \phi_q\frac{\pi}{2}\cot\alpha. \tag{37}$$

Similarly, at the contact perimeter ($r = a$), the potential for the cone is smaller than that for the punch:

$$\phi(a,0) = \phi_q\left(\frac{\pi}{2}\cot\alpha - 1\right). \tag{38}$$

3.3. Spherical indenter

3.3.1. Conducting indenter. From the results presented in Table 1 for the spherical indenter, we recover the classic condition of linear elasticity, $h = 2a^2/D$ for $\phi_0 = 0$. The additional part of the indentation depth is due to displacement induced by the constant potential, ϕ_0, of the indenter.

The conducting spherical indenter shows the same P–a variation as the uncoupled mechanical case. In the case of zero electrical potential ($\phi_0 = 0$), the P–h functional form follows the classic mechanical result, $P \sim h^{3/2}$.

In addition to the electrical potential, the mechanical load also induces an electric charge under the indenter. Note that the electric charge shows a square root singularity at the contact perimeter ($r = a$), as shown in Table 1. The net charge is zero, $Q = 0$, if

$$3\pi\left[\phi_0\left(M_1M_8 - M_2M_7\right) - \left(M_7M_4 - M_8M_3\right)\left(h - \frac{a^2}{R}\right)\right] = -\frac{4a^2}{R}\left(M_7M_4 - M_8M_3\right) \tag{39}$$

indicating that zero net charge under the indenter can be achieved with certain combinations of load, P, and electric potential, ϕ_0.

3.3.2. Insulated indenter. The relation between the penetration depth, h, and the contact radius, a, as well as the P–a relation are exactly the same as for the uncoupled mechanical indentation. The P–h functional form follows the classic mechanics result, $P \sim h^{3/2}$. Because of the absence of an electric potential at the surface, the surface always sinks in: $u_z(a,0) = h/2$.

The maximum potential occurs at the contact center [$\phi_{max} = \phi(0,0)$]: $\phi_{max} = 2\phi_q$. The potential at the contact perimeter is $\phi(a,0) = \phi_{max}/2$.

4. FINITE-ELEMENT SIMULATIONS

The analytical results presented in the preceding sections were also checked with finite-element analyses for four specific piezoelectric materials: two types of lead zirconate titanate, PZT-4 and PZT-5A, and two types of barium titanate, $BaTiO_3$ and 95% $BaTiO_3$–5% $CaTiO_3$. The relevant material properties for these four solids are given in Table 4. A mesh of four-noded, axisymmetric elements was used, with progressively varying element size. The final mesh had 4747 elements and 5058 nodes (Fig. 2). A full Gauss integration scheme was used. The ABAQUS general purpose finite-element program [16] was used with some modifications of the contact conditions. The program had to be supplemented with a subroutine capable of handling the electrical contact boundary conditions employed in this work, i.e. for the electrically conducting or insulated indenters, equations (12) and (13), respectively. For this purpose, line interface elements for the surface of the substrate ($z = 0$) were employed.

Table 4. Piezoelectric properties

Elastic stiffness coefficients (GPa)	PZT-4	PZT-5A	$BaTiO_3$	$(Ba_{0.917}Ca_{0.083})TiO_3$
C_{11}	139.00	121.00	166.00	158.00
C_{33}	115.00	111.00	162.00	150.00
C_{44}	25.60	21.10	42.90	45.00
C_{12}	77.80	75.40	76.60	69.00
C_{13}	74.30	75.20	77.50	67.50
Piezoelectric coefficients (C/m^2)	PZT-4	PZT-5A	$BaTiO_3$	$(Ba_{0.917}Ca_{0.083})TiO_3$
e_{31}	−5.200	−5.400	−4.400	−3.100
e_{33}	15.10	15.80	18.60	13.50
e_{15}	12.70	12.30	11.60	10.90
Dielectric constants (10^{-9} F/m)	PZT-4	PZT-5A	$BaTiO_3$	$(Ba_{0.917}Ca_{0.083})TiO_3$
ϵ_{11}	6.461	8.107	11.151	8.850
ϵ_{33}	5.620	7.346	12.567	8.054

Data from Refs [17, 18].

The mechanical boundary conditions, equations (10) and (11), were adopted from the standard ABAQUS subroutines.

The contact radius, a, was resolved with 24 elements. The outer boundary was at least $20a$ away from the contact regime. The outer boundary conditions were vertically constrained along the sides CD and AB. In addition, sides CD and AB were given zero electrical potential. In all cases, the uncoupled problem ($e_{ij} = 0$) was also solved to verify the accuracy of the simulations with well-known results. The contact stresses were found to be in agreement within 5% error when compared to analytical results, excluding a small region (within an element size) around the cone tip where the analysis predicts a logarithmic singularity that could not be captured by the finite-element analysis.

4.1. Conical indenter

For this case, two materials were analyzed: PZT-4 [lead zirconate titanate $Pb(TiZr)O_3$] and 95% $BaTiO_3$–5% $CaTiO_3$. The stress and electric fields were analyzed for the uncoupled (unpoled) case and for the coupled (poled) case with perfect conductor ($\phi_0 = 0$). The indenter was taken to be rigid, axisymmetric, and of sharp conical apex with the same angle α in all cases. A constant displacement depth, h, was used in all calculations.

For this displacement-controlled conical indentation, the theoretical predictions of normalized indentation force, $P/(\pi a^2 \cot\alpha)$ and the normalized average electric charge distribution, $Q/(\pi a^2 \cot\alpha)$ (see Table 1) are compared with the finite-element results in Table 5. Good agreement was found in all cases, except for the uncoupled force prediction. Here, the logarithmic singularity at the tip of the cone led to a computed pressure distribution which was up to 12% less than that predicted by the theory within one element of the tip. The piezoelectric coupling stiffens the contact response of PZT-4 (by reducing P for fixed h) by 8.8% relative to the uncoupled case. Such stiffening for the 95% Ba_TiO_3–5% $Ca_Ti\ O_3$ is only 2.8%.

4.2. Spherical indenter

For this case, four piezoelectric materials were analyzed: PZT-4, PZT-5A, $BaTiO_3$ and 95% $BaTiO_3$–5% $CaTiO_3$. The sphere was taken to be rigid and part of an axisymmetric paraboloid of the same radius, R, in all cases. For the coupled cases, the sphere was taken either as a perfect conductor with zero electric potential ($\phi_0 = 0$), or as a perfect insulator with no surface electric charge distribution [$q(r) = 0$]. A constant average contact pressure, $P/(\pi a^2) = 33.84$ GPa, was imposed in all calculations.

The numerically predicted normalized applied load, $P/(D^{1/2}h^{3/2})$ and the average normalized electric charge distribution, $Q(D/a^3)$ are tabulated in Table 6, and are compared with the analytical results based on the equations given in Tables 1 and 2. Note that the absence of a mechanical or electrical singularity for the spherical indenter leads to a much better agreement between the analytical and computational results for all four materials and for both the electrical boundary conditions.

The piezoelectric coupling softens the contact response of PZT-4 (relative to the uncoupled case) by 13.7% for the perfect conductor and by 25.4% for the perfect insulator. On the other hand, the piezoelectric coupling stiffens the contact response of 95% $BaTiO_3$–5% $CaTiO_3$ by 8.8% for the perfect conductor and by 1% for the perfect insulator. These predictions have also been confirmed experimentally using spherical indentation [8].

5. CONCLUDING REMARKS

A general theory has been developed for the quantitative indentation of piezoelectric materials by axisymmetric indenters. The theory invokes a transversly isotropic, linear piezoelectric response for the indented solid, while allowing for different electrical boundary conditions which involve electricaly conducting or insulated indenters. A particularly appealing feature of the theory is the indentation force vs the depth of penetration of the indenter into the substrate have been derived in

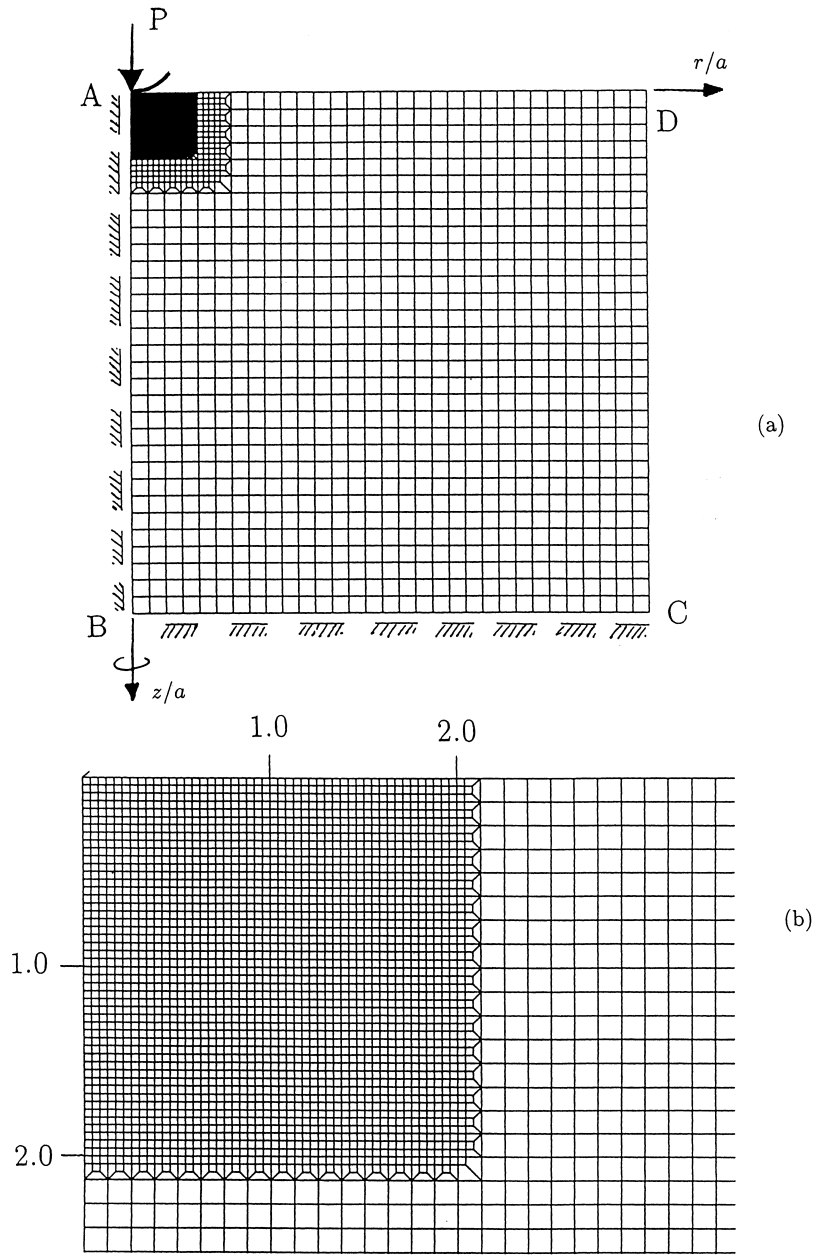

Fig. 2. (a) Overall view of the finite-element mesh used in the present calculations. (b) Details of the mesh close to the contact area.

Table 5. Finite-element (FE) results for conical indenter. The analytical results from Tables 1 and 3 are given within parentheses

Material	Indenter	$P/(\pi a^2 \cos\alpha)$ in GPa FE (Tables 1 and 3)	$Q/(\pi a^2 \cos\alpha)$ in C/m^2 FE (Tables 1 and 3)
PZT-4	uncoupled	4.98 (5.58)	0.00 (0.00)
	conductor	4.37 (4.57)	10.95 (10.5)
95% $BaTiO_3$–5% $CaTiO_3$	uncoupled	7.90 (7.99)	0.00 (0.00)
	conductor	8.12 (8.36)	8.80 (8.40)

Table 6. Finite-element (FE) results for spherical indenter. The analytical results from Tables 1–3 are given within parentheses

Material	Indenter	$P/(D^{1/2}h^{3/2})$ in GPa FE (Tables 1–3)	$Q(D/a^3)$ in C/m^2 FE (Tables 1–3)
PZT-4	uncoupled	105.14 (104.30)	0.00 (0.00)
	conductor	86.16 (91.50)	17.84 (18.60)
	insulator	75.06 (80.60)	0.00 (0.00)
PZT-5A	conductor	67.63 (68.54)	32.36 (33.02)
	insulator	58.95 (60.02)	0.00 (0.00)
$BaTiO_3$	uncoupled	121.23 (119.75)	0.00 (0.00)
	conductor	124.03 (124.92)	14.44 (14.87)
	insulator	122.78 (122.90)	0.00 (0.00)
95% $BaTiO_3$–5% $CaTiO_3$	uncoupled	150.69 (148.90)	0.00 (0.00)
	conductor	157.28 (153.10)	14.34 (15.00)
	insulator	157.88 (154.00)	0.00 (0.00)

closed form for flat-ended cylindrical punch, circular cone and spherical indenters, in a manner whereby direct connections can be made with experimental measurements. It has been demonstrated that the electric charge or potential at the contacting surface plays an important role in determining the resistance to indentation. The surface values of contact stresses, as well as the electrical potential and charges during quasi-static indentation were found explicitly. The mechanical and electrical fields below the surface were also computed. Our analysis also reveals that the electro-mechanical coupling can also significantly alter the pile-up or sink-in of the material around the indenter even in the absence of any inelastic deformation processes. Key predictions of the theory have been substantiated with finite-element simulations.

The above analysis provides a scientific basis for the interpretation of indentation experiments on piezoelectric materials which, as shown in our companion work [8, 9], have many potential applications for property and microstructural characterization. Instrumented indentation can be a quick and inexpensive preliminary test for quality control in commercial production. In many cases, indentation may be the only method for testing small volumes of materials such as in thin films, layered plates or composites. On the basis of the present analysis, it is shown in Refs [8, 9] that a continuous record of force–depth and force–potential signals could lead to the determination of individual or combined material properties such as elastic moduli, dielectric and piezoelectric constants for polycrystalline or monocrystalline materials with up to six-fold symmetry. Indentation can also assess effects such as loss of piezoelectricity due to aging during service or storage. As an actuator mechanism, indentation can serve as a microelectric generator, or as "skin" actuator for contact devices or micromotors. Conical or spherical indentation can model contact-induced damage.

REFERENCES

1. Hertz, H., *J. reinen angewandte Mathematik*, 1882, **92**, 156.
2. Johnson, K.-L., *Contact Mechanics*. Cambridge University Press, Cambridge, 1985.
3. Gladwell, M.L., *Contact Problems in the Classical Theory of Elasticity*. Sijthoff and Noordhoff, The Netherlands, 1980.
4. Uchino, K., *Piezoelectric Actuators and Ultrasonic Motors*. Kluwer, Boston, 1997.
5. Suresh, S., Alcala, J. and Giannakopoulos, A.E., MIT Case No. 7280, Technology Licensing Office, MIT, U.S. Patent Application pending, 1996.
6. Giannakopoulos, A.E. and Suresh, S., *Scripta mater.*, 1999, in press.
7. Oliver, W.C. and Pharr, G.M., *J. Mater. Res.*, 1992, **7**, 1564.
8. Ramamurty, U., Sridhar, S., Giannakopoulos, A.E. and Suresh, S. S., *Acta mater.*, 1999, in press.
9. Sridhar, S., Giannakopoulos, A.E., Suresh, S. and Ramamurty, U., *J. appl. Phys.*, 1999, **85**, 350.
10. Matysiak, S., *Bull. Polish Acad. Sci. (Tech. Sci.)*, 1985, **33**, 25.
11. Sneddon, I.N., *Special Functions of Mathematical Physics and Chemistry*. Longman, London, 1980.
12. Ding, H., Chen, B. and Liang, J., *Int. J. Solids Struct.*, 1996, **33**, 2283.
13. Hanson, M.T., *J. appl. Mech.*, 1992, **59**, S123.
14. Dahan, M. and Zarka, J., *Int. J. Solids Struct.*, 1977, **13**, 229.
15. Sneddon, I.N., *Mixed Boundary Problems in Potential Theory*. North Holland, Amsterdam, 1996.
16. ABAQUS, Finite element code, Version 5.5, Hibbit, Karlsson and Sorensen, Inc., Pawtucket, RI, 1996.
17. Jaffe, B., Cook, W.R. and Jaffe, H., *Piezoelectric Ceramics*. Academic Press, New York, 1971.
18. Bechmann, R., *J. Acoust. Soc. Am.* **28**, 347.

APPENDIX A

Constants used in the analysis

$$m_1 = e_{15}\gamma_1 - c_{44}(k_1\alpha_1 + \beta_1) \tag{A.1}$$

$$m_2 = e_{15}\gamma_{21} - c_{44}(\delta\alpha_{21} - \omega\alpha_{22} + \beta_{21}) \tag{A.2}$$

$$m_3 = e_{15}\gamma_{22} - c_{44}(\delta\alpha_{22} + \omega\alpha_{21} + \beta_{22}) \tag{A.3}$$

$$m_4 = -\epsilon_{11}\gamma_1 - e_{15}(k_1\alpha_1 + \beta_1) \tag{A.4}$$

$$m_5 = -\epsilon_{11}\gamma_{21} - e_{15}(\delta\alpha_{21} - \omega\alpha_{22} + \beta_{21}) \tag{A.5}$$

$$m_6 = -\epsilon_{11}\gamma_{22} - e_{15}(\delta\alpha_{22} + \omega\alpha_{21} + \beta_{22}) \tag{A.6}$$

$$M_1 = \beta_1 - \beta_{22}\frac{m_1}{m_3} \tag{A.7}$$

$$M_2 = \beta_{21} - \beta_{22}\frac{m_2}{m_3} \tag{A.8}$$

$$M_3 = \gamma_1 - \gamma_{22}\frac{m_1}{m_3} \tag{A.9}$$

$$M_4 = \gamma_{21} - \gamma_{22}\frac{m_2}{m_3} \tag{A.10}$$

$$M_5 = \frac{m_1}{k_1} - \frac{m_3\delta - m_2\omega}{\delta^2 + \omega^2}\left(\frac{m_1}{m_3}\right) \tag{A.11}$$

$$M_6 = \frac{m_2\delta + m_3\omega}{\delta^2 + \omega^2} - \frac{m_3\delta - m_2\omega}{\delta^2 + \omega^2}\left(\frac{m_2}{m_3}\right) \tag{A.12}$$

$$M_7 = \frac{m_4}{k_1} - \frac{m_6\delta - m_5\omega}{\delta^2 + \omega^2}\left(\frac{m_1}{m_3}\right) \tag{A.13}$$

$$M_8 = \frac{m_5\delta + m_6\omega}{\delta^2 + \omega^2} - \frac{m_6\delta - m_5\omega}{\delta^2 + \omega^2}\left(\frac{m_2}{m_3}\right) \tag{A.14}$$

$$M_9 = \alpha_1 - \alpha_{22}\frac{m_1}{m_3} \tag{A.15}$$

$$M_{10} = \alpha_{21} - \alpha_{22}\frac{m_2}{m_3} \tag{A.16}$$